IEEE Access
Multidisciplinary ⋮ Rapid Review ⋮ Open Access Journal

Received November 1, 2020, accepted November 21, 2020, date of publication November 25, 2020,
date of current version December 9, 2020.

Digital Object Identifier 10.1109/ACCESS.2020.3040620

An Optimized Hybrid Fractional Order Controller for Frequency Regulation in Multi-Area Power Systems

EMAD A. MOHAMED[1], EMAD M. AHMED[2,3], (Senior Member, IEEE), AHMED ELMELEGI[1], MOKHTAR ALY[1,4], (Member, IEEE), OSAMA ELBAKSAWI[2,5], AND AL-ATTAR ALI MOHAMED[1]

[1]Department of Electrical Engineering, Faculty of Engineering, Aswan University, Aswan 81542, Egypt
[2]Department of Electrical Engineering, Jouf University, Sakaka 2014, Saudi Arabia
[3]AWCRC, Faculty of Engineering, Aswan University, Aswan 81542, Egypt
[4]Electronics Engineering Department, Universidad Tecnica Federico Santa Maria, Valparaiso 2390123, Chile
[5]Department of Electrical Engineering, Faculty of Engineering, Port-Said University, Port Fuad 42526, Egypt

Corresponding author: Emad M. Ahmed (emad@eng.aswu.edu.eg)

The authors extend their appreciation to the Deputyship for Research & Innovation, Ministry of Education in Saudi Arabia for funding this work through the project number "375213500". The authors also would like to extend their sincere appreciation to the central laboratory at Jouf University for support this study. This work is also supported in part by SERC Chile (ANID/FONDAP15110019) and by AC3E (ANID/Basal/FB0008).

ABSTRACT Multi-area power systems inhere complicated nonlinear response, which results in degraded performance due to the insufficient damping. The main causes of the damping problems are the stochastic behavior of the renewable energy sources, loading conditions, and the variations of system parameters. The load frequency control (LFC) represents an essential element for controlling multi-area power systems. Therefore, the proper design of the controllers is mandatory for preserving reliable, stable and high-quality electrical power. The controller has to suppress the deviations of the area frequency in addition to the tie-line power. Therefore, this paper proposes a new frequency regulation method based on employing the hybrid fractional order controller for the LFC side in coordination with the fractional order proportional integral derivative (FOPID) controller for the superconducting energy storage system (SMES) side. The hybrid controller is designed based on combining the FOPID and the tilt integral derivative (TID) controllers. In addition, the controller parameters are optimized through a new application of the manta ray foraging optimization algorithm (MRFO) for determining the optimum parameters of the LFC system and the SMES controllers. The optimally-designed controllers have operated cooperatively and hence the deviations of the area frequency and tie-line power are efficiently suppressed. The robustness of the proposed controllers is investigated against the variation of the power system parameters in addition to the location and/or magnitude of random/step load disturbances.

INDEX TERMS Fractional order controller, load frequency control, manta ray foraging optimization, multi-area power systems, renewable energy sources, superconducting energy storage systems.

I. INTRODUCTION

Worldview change toward more practical power systems has increased the concerns of renewable energy generations. Currently, renewable energy covers about 14% of the load demand around the world [1]. Lately, high penetration levels of renewable energy sources (RESs) have been installed in electrical power systems. Although, these RESs are continuously fluctuating, and their output power is highly dependent on the environmental conditions, such as ambient temperature, solar irradiance, wind speed, etc. In addition, the connected electrical loads are stochastic and the electrical power demand is continuously changing. Therefore, perpetual imbalance among the load demand and the generated power is always existing in the interconnected power systems, which affects the system stability and leads to deviations in the area frequency and fluctuations in the tie-line power beyond the scheduled values [2].

Modern control and operation of power systems are developed based on a decentralized pattern instead of the

The associate editor coordinating the review of this manuscript and approving it for publication was Tariq Masood.

traditional centralized systems. Load frequency control (LFC) of the interconnected multi-area power systems represents the main part of the automatic generation controller (AGC). The LFC is responsible for regulating the generated electrical power to mitigate the load demand variations, parametric uncertainties, RESs fluctuations, transient disturbances of the plant, etc. The preliminary control activities of the LFC are performed through the speed governor. However, it does not represent enough mean to precisely mitigate the consistent oscillations due to the imbalance between the generation and the demand loads. Thence, supplementary controllers are required to keep the steady state area frequency deviations and tie-line power at zero values [3].

In the literature, several featured intelligent techniques have been proposed for LFC functionality, such as the robust control systems [4], [5], internal model controllers (IMC) [6], sliding mode controllers [7], adaptive controllers [8], intelligent control systems [9], linear matrix inequalities controllers [10], etc. In addition, fuzzy logic controllers [11], variable structure controllers [12], model-predictive controllers [13], disturbance rejection controllers have been also proposed for performing various LFC functions [14]. Moreover, data-driven controllers have been proposed for the cooperative control of area frequency in multi-area power systems [15]. In data-driven controllers, the control criterion is directly optimized based on the measured system response. In [16], a reinforcement learning algorithm is presented without the necessity for full communication among the controllers while achieving cooperative control action. As well, deep reinforcement learning algorithms have been introduced for single area power systems [17]. However, they require more complex computations, data learning procedure, and expert knowledge.

Although intelligent control strategies can successfully handle the frequency stability problems, they exhibit several limitations linked to the increased computational complexity, and the requirement for deep learning procedure and powerful inference tool. Thence, several industrial applications are still utilizing many classical linear and nonlinear control methods, which have been employed for LFC function in electrical power systems due to their simplicity in structure and their economical cost compared to other control techniques [18]. The main control structures are the integral, proportional integral (PI) controller, proportional integral derivative (PID) controller, PID with the derivative filter (PIDF) [19], [20], two-degree-of-freedom PID (2-DoF-PID) controller [21], cascaded PD-PID controller [22], PID with second order derivatives (PID2D) controller [23], fuzzy-logic PI (FL-PI), fuzzy-logic PID (FL-PID) [24], neuro-fuzzy based controllers [25], and linear active disturbance rejection control (LADRC) [26].

Recently, the tilt integral derivative controller (TID) has been addressed to LFC. Its transfer function is more closely to the optimal one, where improved feedback is achieved [27]. The derivative part in TID ensures the fast response of the controller and improves the system stability. Moreover, a high pass filter is equipped with the derivative term to reduce the effect of any input noise on system stability [28]. Moreover, the fractional order (FO) based controllers have been also presented in the literature including the fractional order PID (FOPID) [29], fuzzy fractional order PI and PD controller (FL-FOPI-FOPD) [30], fuzzy with FOPIDF (FL-FOPIDF) [31], combined fuzzy PIDF and FOI (FL-PIDF-FOI) [32], hybrid [27], etc. Hence, the family of PID controller, FO, and their extensions based expanded controllers are widely preferred in LFC thanks to their simplicity, robustness, and efficiency. Moreover, they have shown an improved dynamic performance regarding reference to the tracking and disturbance rejection functions. In addition, this family of controllers can provide an optimized and powerful response for wide operating ranges for various processes, including nonlinear and stable/unstable processes. However, these types of controllers are more sensitive to system uncertainties, especially with the recent situation of modern power systems, which become more severe when considering system uncertainties, physical limitations, and fluctuations of RESs and load variations. The stable and efficient operation of the LFC is determined by adequate selection for the controller parameters. Therefore, it is crucial to design the optimal parameters of PID, FO controllers and their families to be able to withstand any system variations.

The complexity of the design process of the controller parameters is depending on the design procedures among the existing tuning techniques. Normally, the controller parameters can be set by either classical methods, artificial intelligence methods or meta-heuristic optimization algorithms [33]. In the classical methods, the design of the optimal controller parameters is based on using complex mathematical models and calculations, which adds more difficulties for the design process. In artificial intelligence-based methods, the design process depends on the training data and analysis for determining the optimal parameters of the controller. From another side, the meta-heuristic based algorithms have found great concerns for determining the optimal controller parameters through proper tuning of various parameters [20], [34].

Several optimization algorithms have been presented in the literature, wherein the classical genetic algorithm (GA) and particle swarm optimization (PSO) methods are the most widely applied techniques [33]. Many other techniques have been reported in the literature, such as salp swarm algorithm (SSA) [34], differential evolution (DE) [20], firefly algorithm (FA) [35], teaching learning-based optimization (TLBO) [21], ant-lion optimizer algorithm (ALO) [23], imperialist competitive algorithm (ICA) [36], etc. In addition, hybrid and combined optimization techniques have been addressed in the literature for designing the controller parameters. However, some of these algorithms suffer from long elapsed time, stagnation, and being very sensitive to their parameters. Others can successfully present a good performance as their objective functions have the capability of weighting the output signals in different

objectives simultaneously. However, they suffer from long computational time and need frequent iterations to assure solution convergence.

Recently, the continuous development of computational swarm optimization algorithms exemplifies great motivation for the authors to apply the new manta ray foraging optimization algorithm (MRFO) for determining the optimum parameters of the LFC and the SMES controllers. MRFO is a novel optimization algorithm that has been originally developed in [37]. The MRFO has many advantages over other swarm algorithms, such as: (i) Ability to avoid the trap in local minima, (ii) Higher accuracy, (iii) Achieving fast convergence characteristics, (iv) Lower computational cost and higher performance, (v) lowest control parameters to be adjusted. To the best knowledge of the authors, the MRFO algorithm has not been applied so far for the LFC problem of an interconnected power system. Therefore, this work utilizes, for the first time, the MRFO to optimally design the proposed controllers.

It is clear from the above discussion that several control structures with different optimization techniques have been addressed in the literature, and the dynamic performance of the LFC is dependent on the optimization technique, and the controller structure as well. Moreover, the effect of the combination of the (FOPID) and the tilt integral derivative (TID) controllers has not been tackled in the literature for LFC. In this context, this paper proposes a new frequency regulation controller based on the hybrid FOPID-TID controller for the LFC side in coordination with the FOPID controller for SMES side in a multi-area power system. This new application of the hybrid controller has cooperated with the aid of SMES as an energy storage source based on the FOPID controller to smoothly damp out the deviations of the areas frequencies and tie-line power. In addition, the MRFO is used to tune all controller parameters in each area. the main contribution of this paper can be summarized as follows:

- A new frequency regulation method using the hybrid controller is proposed for the LFC side in this paper, which is based on the combination of FOPID and TID controllers.
- An enhanced cooperation is proposed between the proposed hybrid controller for LFC and the FOPID controller for the SMES as an energy storage source to smoothly mitigate the areas frequency deviations and the-line power fluctuations.
- A new application of the MRFO method for tuning the proposed hybrid controller and the SMES controller is proposed. The proposed method eliminates the need for large training data and complex mathematical calculations.
- A new employment of the hybrid controller in the LFC loop in an interconnected power system as well as the utilizing of the MRFO to select the parameters of the cooperative hybrid and SMES FOPID controllers are presented in the paper.

The remaining of the paper is organized as follows; Section II presents the mathematical modelling of the selected two area power system and the modelling of the RESs and SMES system. Section III introduces the fractional order mathematical modelling and the proposed hybrid controller. The optimization problem and the proposed MRFO method details are presented in Section IV. Section V provides the obtained simulation results of the two are power system. The discussions and the performance comparison are presented in Section VI. Finally, Section VII provides the conclusion of the paper.

II. MATHEMATICAL MODELLING OF THE STUDIED MULTI-AREA POWER SYSTEM

In order to validate the effectiveness of the proposed controller, a two-area, namely area a and area b, an interconnected power system model is considered as a case study. Fig. 1 shows the schematic diagram of the studied system and the main components in each area. Area (a) consists of a thermal power plant, wind energy unit, SMES storage unit, and local loads. Whereas, area (b) includes a hydraulic power station, PV energy unit, SMES storage, and local loads as well. Throughout the abnormal conditions, the frequency deviations between the two areas are used to derive the exchanged tie-line power between the two-area power system. The proposed hybrid controller has to handle both the frequency deviation in each area in addition to the tie-line power exchange to overcome the power mismatch and to enhance system stability. Moreover, the studied system contains SMES energy units for further improving the frequency stability by providing the virtual inertia emulation functionality in the studied system. Fig. 2 shows the dynamical modelling of the various elements in the studied two-area power system. All the parameters of the studied system are provided in Table 1 according to the provided system data in [38].

The transfer function of the thermal power plant governor $G_g(s)$ and the turbine $G_t(s)$ for area a are modelled as follows in [39]:

$$G_g(s) = \frac{1}{T_g s + 1} \tag{1}$$

$$G_t(s) = \frac{1}{T_t s + 1} \tag{2}$$

The general transfer function of hydro turbine is comprised of governor, droop compensation and penstock turbine. It can be represented as follows in [38]:

$$G_h(s) = \frac{1}{T_1 s + 1} \cdot \frac{T_R s + 1}{T_2 s + 1} \cdot \frac{-T_w s + 1}{0.5 T_w s + 1} \tag{3}$$

whereas, the microgrid power system transfer function $G_{px}(s)$ is modeled as follows in [39]:

$$G_{px}(s) = \frac{1}{2H_x s + D_x} \tag{4}$$

where, x denotes to the studied area (where $x \in \{a, b\}$). The transfer function of the wind generation $G_{WT}(s)$ for area a and

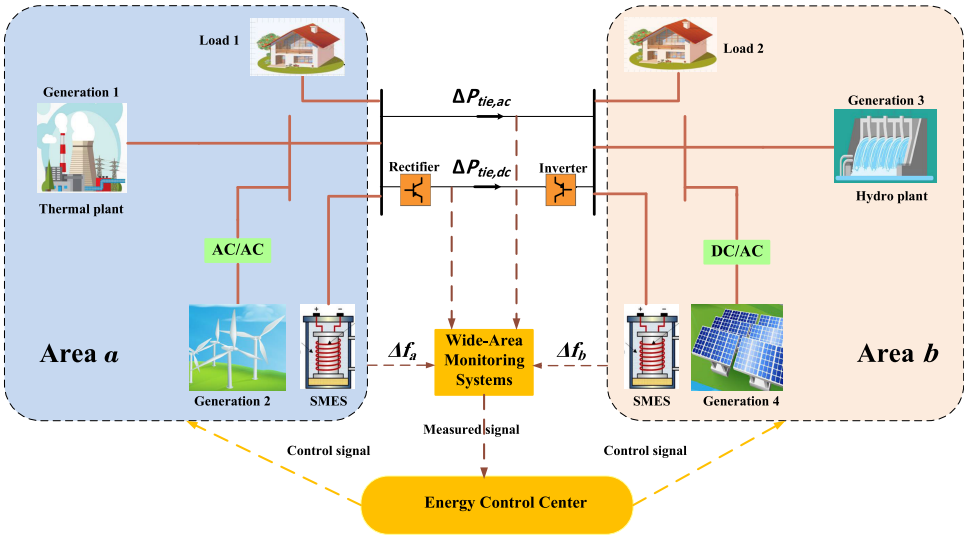

FIGURE 1. Single line diagram of the studied two-area interconnected power system case study.

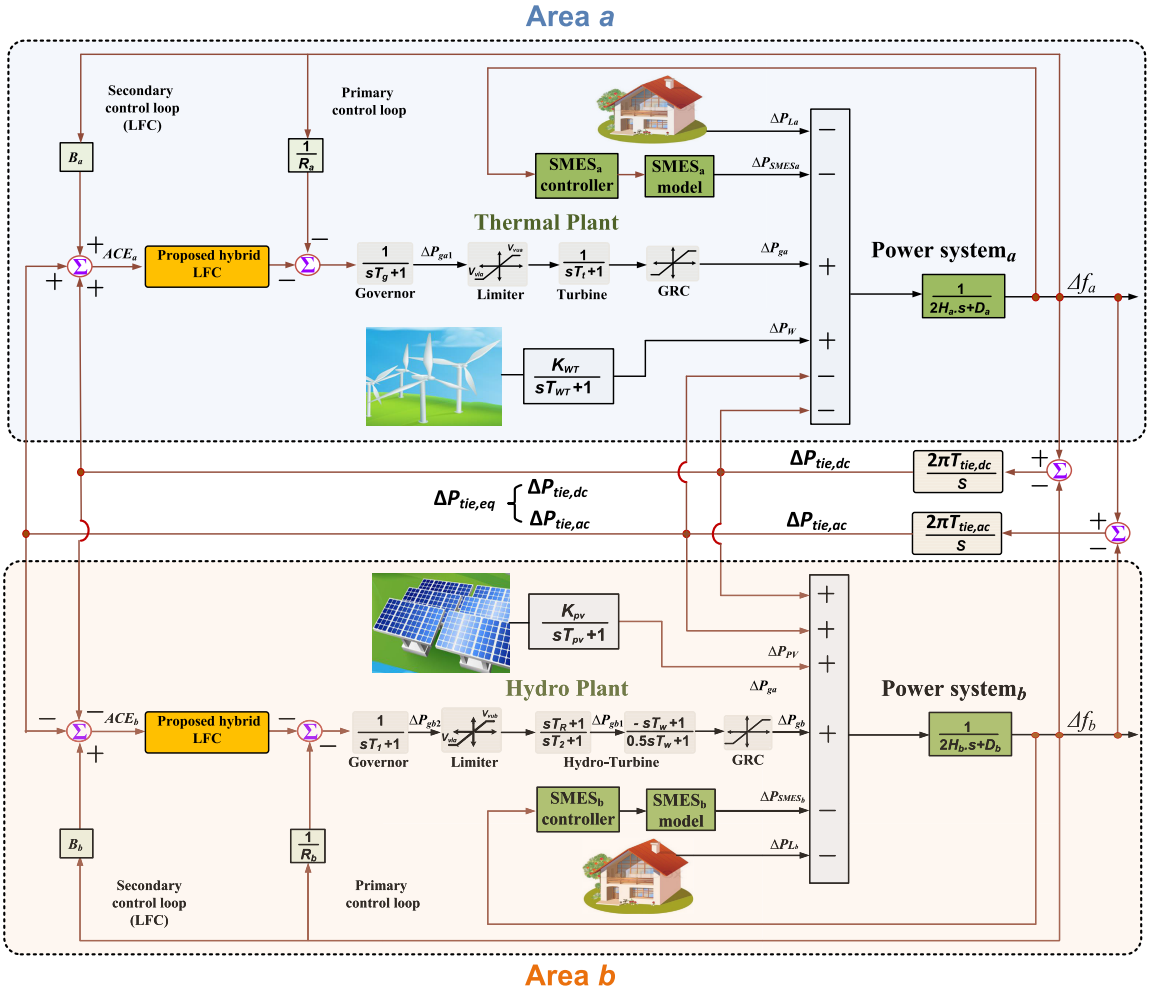

FIGURE 2. The overall structure and system modelling of the studied two-area interconnected power system.

TABLE 1. Main parameters for the studied system ($x \in \{a, b\}$), [38].

Parameter	Symbol	Values	
		area a	area b
Area rated capacity	P_{rx} (MW)	1200	1200
Droop constant	R_x (Hz/MW)	2.4	2.4
Frequency bias value	B_x (MW/Hz)	0.4249	0.4249
Minimum limit of valve gate	V_{vlx} (p.u.MW)	-0.5	-0.5
Maximum limit of valve gate	V_{vux} (p.u.MW)	0.5	0.5
Time constant of thermal governor	T_g (s)	0.08	-
Time constant of thermal turbine	T_t (s)	0.3	-
Time constant of hydraulic governor	T_1 (s)	-	41.6
Transient droop time constant of hydraulic governor	T_2 (s)	-	0.513
Reset time of hydraulic governor	T_R (s)	-	5
Water starting time of hydro turbine	T_w (s)	-	1
Power system inertia constant	H_x (p.u.s)	0.0833	0.0833
Power system damping coefficient	D_x (p.u./Hz)	0.00833	0.00833
Time constant of PV	T_{PV} (s)	-	1.3
Gain of PV	K_{PV} (s)	-	1
Time constant of wind	T_{WT} (s)	1.5	-
Gain of wind	K_{WT} (s)	1	-
Converter time constant of SMES	T_{DCx} (s)	0.03	0.03
coil of SMES	L_x (H)	0.03	0.03
Control gain of SMES	K_{SMESx} (kV/unit MW)	100	100
Control gain	K_{Idx} (kV/kA)	0.2	0.2
Inductor rated current of SMES	I_{d0x} (kA)	4.5	4.5
Two area capacity ratio	A_{ab}	-1	
Sync. coefficient of HVDC	$T_{tie,dc}$ (s)	0.1732	
Sync. coefficient of HVAC	$T_{tie,ac}$ (s)	0.0865	

the PV generation $G_{PV}(s)$ for area b are modelled as follows in [39]:

$$G_{WT}(s) = \frac{K_{WT}}{T_{WT}s + 1} \tag{5}$$

$$G_{PV}(s) = \frac{K_{PV}}{T_{PV}s + 1} \tag{6}$$

In the studied system, a more practical SMES model is considered based on the presented model in [39]. The different parameters and symbols definitions are included in Table 1 for the various elements in the two-area system. In the analysis, the equivalent tie-line power deviation $\Delta P_{tie,eq}$ is employed to consider the total equivalent tie-line power deviations of the HVDC tie-line $\Delta P_{tie,dc}$ and the HVAC tie-line $\Delta P_{tie,ac}$. The thermal unit has a generation constraint GRC of 10%/min and the hydro unit has 270%/min for rising and 360%/min for lowering generation as considered in the literature in [38].

The various models are combined in order to provide a complete representation of the studied system. In which, the various models of the generation and load demands are utilized for deriving dynamic equations of the considered case study. Afterward, the state-space model for describing the studied power system is considered. In the state-space model, x, y, ω and u denote the vectors that represent the system state variables, output states, various disturbances, and the control variables, respectively. The control variables of the studied system include the ACE signals in the two-area (ACE_a and ACE_b), in addition to the output power deviation of the two considered SMES devices (ΔP_{SMES_a} and ΔP_{SMES_b}). Whereas, A, B_1, B_2, and C denote to the corresponding parameters matrices for the linearized state-space model of the system. The state-space model and parameters can be represented as follows (7)–(14), shown at the bottom of the next page.

III. THE PROPOSED FO HYBRID CONTROLLER STRUCTURE

A. FRACTIONAL ORDER CALCULUS

The recent advancements in the fractional order calculus have enabled researchers and designers to utilize fractional order operators in several fields [40], [41]. Particularly, more precise modelling and/or controller design of processes can be achieved in various applications of control engineering. The fractional operators can lead to more robustness and increased applicability in the controller design. The utilization of the integral and/or differential based fractional operators instead of integer order operators has provided more flexibility in the controller design process.

In general, the FO operator is represented by ${}_{t_0}D^{\alpha}_{t_f}$, where, t_0 and t_f represent the time limits for calculating the operator, and α denotes to the order for the FO operator [42]. The FO operator can take several forms as follows:

$${}_{t_0}D^{\alpha}_{t_f} = \begin{cases} \alpha > 0 \rightarrow \dfrac{\mathrm{d}^{\alpha}}{\mathrm{d}t^{\alpha}} \\ \alpha < 0 \rightarrow \displaystyle\int_{t_0}^{t_f} \mathrm{d}t^{\alpha} \\ \alpha = 0 \rightarrow 1 \end{cases} \tag{15}$$

Several approaches can be employed for designing the FO integral and differentiator operators. The main methods for defining FO operators are the Riemann-Liouville, Caputo, and Grunwald-Letkinov methods [40]. The time domain-based implementations for FO operators require complicated mathematical calculations. In this context, several approximate representations have been introduced, such

as Oustaloup, Carlson, Matsuda, Chareff, and the continued fractional expansion [43]. These approximation methods can represent the FO operators/transfer functions with integer-based operators/transfer functions. In this work, the Oustaloup approximation method is utilized for representing the FO operators. In the proposed design method, the design of band-pass filter is proposed for certain frequency range $[\omega_{\text{fbl}}, \omega_{\text{fbu}}]$, where ω_{fbl} and ω_{fbu} are the lower and upper values of the frequency bounds, respectively. The approximate transfer function for s^{λ} with $\lambda \in \Re$ is expressed by integer order equivalent transfer functions with poles, zeros, and gains as follows [42]:

$$s^{\lambda} \approx K \prod_{k=-M}^{M} \frac{s+\omega_{\text{k}}^{\text{z}}}{s+\omega_{\text{k}}^{\text{p}}} \tag{16}$$

$$\dot{x} = Ax + B_1\omega + B_2\, u \tag{7}$$

$$y = Cx \tag{8}$$

$$x = \left[\begin{array}{cccccccccc} \Delta f_a & \Delta P_{ga} & \Delta P_{ga1} & \Delta P_{WT} & \Delta f_b & \Delta P_{gb} & \Delta P_{gb1} & \Delta P_{gb2} & \Delta P_{PV} & \Delta P_{tie,eq} \end{array}\right]^T \tag{9}$$

$$\omega = \left[\begin{array}{cccc} \Delta P_{la} & P_{WT} & \Delta P_{lb} & P_{PV} \end{array}\right]^T \tag{10}$$

$$u = \left[\begin{array}{cccc} ACE_a & \Delta P_{SMES_a} & ACE_b & \Delta P_{SMES_b} \end{array}\right]^T \tag{11}$$

$$A = \left[\begin{array}{cccccccccc} -\frac{D_a}{2H_a} & \frac{1}{2H_a} & 0 & \frac{1}{2H_a} & 0 & 0 & 0 & 0 & 0 & -\frac{1}{2H_a} \\ 0 & -\frac{1}{T_t} & \frac{1}{T_t} & 0 & 0 & 0 & 0 & 0 & 0 & 0 \\ -\frac{1}{R_aT_g} & 0 & -\frac{1}{T_g} & 0 & 0 & 0 & 0 & 0 & 0 & 0 \\ 0 & 0 & 0 & -\frac{1}{T_{WT}} & 0 & 0 & 0 & 0 & 0 & 0 \\ 0 & 0 & 0 & 0 & -\frac{D_b}{2H_b} & \frac{1}{2H_b} & 0 & 0 & \frac{1}{2H_b} & \frac{1}{2H_b} \\ 0 & 0 & 0 & 0 & \frac{2T_R}{R_bT_1T_2} & -\frac{2}{T_w} & \frac{2T_2+2T_w}{T_2T_w} & \frac{2T_R-2T_1}{T_1T_2} & 0 & 0 \\ 0 & 0 & 0 & 0 & -\frac{T_R}{R_bT_1T_2} & 0 & -\frac{1}{T_2} & \frac{T_1-T_R}{T_1T_2} & 0 & 0 \\ 0 & 0 & 0 & 0 & -\frac{1}{R_bT_1} & 0 & 0 & -\frac{1}{T_1} & 0 & 0 \\ 0 & 0 & 0 & 0 & 0 & 0 & 0 & 0 & -\frac{1}{T_{PV}} & 0 \\ 2\pi T_{tie,eq} & 0 & 0 & 0 & -2\pi T_{tie,eq} & 0 & 0 & 0 & 0 & 0 \end{array}\right] \tag{12}$$

$$B_1 = \left[\begin{array}{cccc} -\frac{1}{2H_a} & 0 & 0 & 0 \\ 0 & 0 & 0 & 0 \\ 0 & 0 & 0 & 0 \\ 0 & \frac{K_{WT}}{T_{WT}} & 0 & 0 \\ 0 & 0 & -\frac{1}{2H_b} & 0 \\ 0 & 0 & 0 & 0 \\ 0 & 0 & 0 & 0 \\ 0 & 0 & 0 & 0 \\ 0 & 0 & 0 & \frac{K_{PV}}{T_{PV}} \\ 0 & 0 & 0 & 0 \end{array}\right], \quad \text{and } B_2 = \left[\begin{array}{cccc} 0 & -\frac{1}{2H_a} & 0 & 0 \\ 0 & 0 & 0 & 0 \\ -\frac{1}{T_g} & 0 & 0 & 0 \\ 0 & 0 & 0 & 0 \\ 0 & 0 & 0 & -\frac{1}{2H_b} \\ 0 & 0 & \frac{2T_R}{T_1T_2} & 0 \\ 0 & 0 & -\frac{T_R}{T_1T_2} & 0 \\ 0 & 0 & -\frac{1}{T_1} & 0 \\ 0 & 0 & 0 & 0 \\ 0 & 0 & 0 & 0 \end{array}\right] \tag{13}$$

$$C = \left[\begin{array}{cccccccccc} 1 & 0 & 0 & 0 & 0 & 0 & 0 & 0 & 0 & 0 \\ B_a & 0 & 0 & 0 & 0 & 0 & 0 & 0 & 0 & 1 \\ 0 & 0 & 0 & 0 & 1 & 0 & 0 & 0 & 0 & 0 \\ 0 & 0 & 0 & 0 & B_b & 0 & 0 & 0 & 0 & -1 \end{array}\right] \tag{14}$$

$$\omega_{\mathrm{k}}^{\mathrm{z}} = \omega_{\mathrm{fbl}}\left(\frac{\omega_{\mathrm{fbu}}}{\omega_{\mathrm{fbl}}}\right)^{\frac{k+M+\frac{1-\lambda}{2}}{2M+1}} \tag{17}$$

$$\omega_{\mathrm{k}}^{\mathrm{p}} = \omega_{\mathrm{fbl}}\left(\frac{\omega_{\mathrm{fbu}}}{\omega_{\mathrm{fbl}}}\right)^{\frac{k+M+\frac{1+\lambda}{2}}{2M+1}} \tag{18}$$

$$K = \left(\frac{\omega_{\mathrm{fbu}}}{\omega_{\mathrm{fbl}}}\right)^{\frac{-\lambda}{2}} \prod_{k=-M}^{M} \frac{\omega_{\mathrm{k}}^{\mathrm{p}}}{\omega_{\mathrm{k}}^{\mathrm{z}}} \tag{19}$$

where, $\omega_{\mathrm{k}}^{\mathrm{p}}$ and $\omega_{\mathrm{k}}^{\mathrm{z}}$ represent the poles and zeros for the sequence k. The approximate transfer function of the FO operator contains $(2M+1)$ number of poles and zeros. In the current study, the order of Oustaloup method is selected $(M = 5)$ with frequency range of $\omega \in [\omega_{\mathrm{fbl}}, \omega_{\mathrm{fbu}}]$ and it is selected in the range of $[-1000, 1000]$ rad/s.

B. FRACTIONAL ORDER CONTROLLERS

In general, integer PID controllers are widely employed for several industrial applications due to their simple design and structure. Fig. 3a shows the block diagram of integer type PID controller. The transfer function of PID controller can be represented as follows:

$$C(s) = \frac{Y(s)}{E(s)} = K_p + \frac{K_i}{s} + K_d\, s \tag{20}$$

where, K_p, K_i and K_d denote to the proportional, integral and differential gains for the PID controller. Although the integer PID controllers provide simple solutions, they are subjected to lose their high performance in case of disturbances. Therefore, concerns have been directed to various robust and intelligent controllers for LFC systems. From another side, the FO versions of PID controllers have attracted much concerns. Fig. 3b shows the block diagram of the FOPID controller. The transfer function of FOPID controller can be represented as following:

$$C(s) = \frac{Y(s)}{E(s)} = K_p + \frac{K_i}{s^{\lambda}} + K_d\, s^{\mu} \tag{21}$$

where, λ, and μ represent the FO operators and they are often tuned in the range of $[0, 1]$. The FOPID controllers have shown more flexibility and wide range dealing of disturbances. FOPID controllers can simultaneously handle several multi objectives for wide dynamic operating range compared to integer-based PID controllers.

Additionally, another version of FO controllers has been utilized in the literature using the tilt integral derivative (TID) controller. The mathematical model of the TID controller can be represented as follows:

$$C(s) = \frac{Y(s)}{E(s)} = K_t\, s^{-(\frac{1}{n})} + \frac{K_i}{s} + K_d\, s \tag{22}$$

where, n denotes to FO operator for the tilt component. The tilt component can provide more simple tuning process, enhancement of disturbance rejection capability and improved robustness to parameters uncertainty.

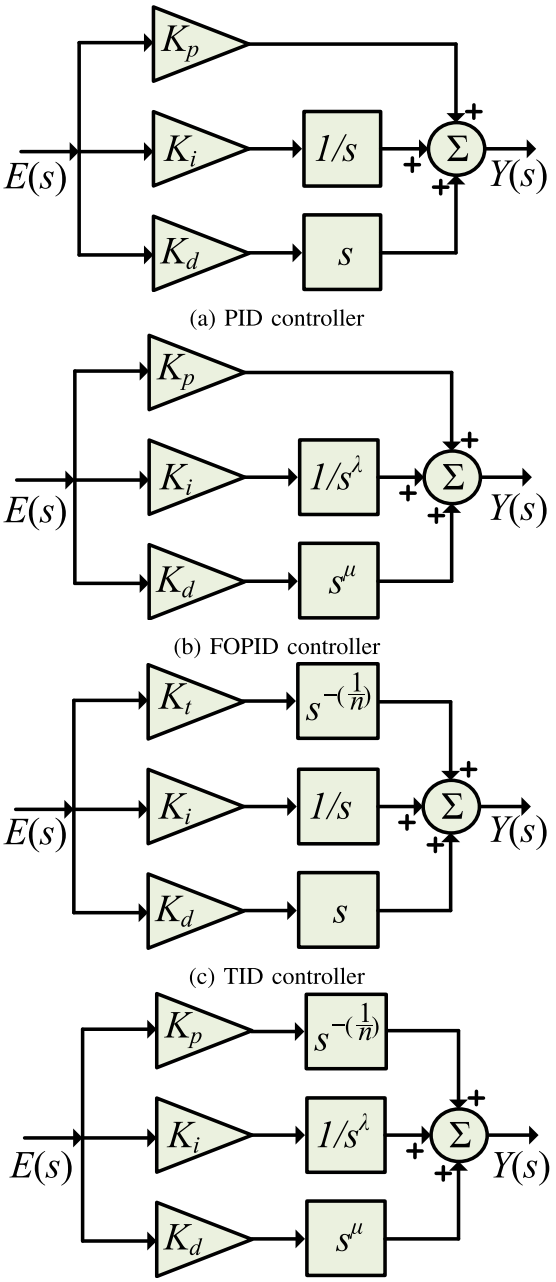

(a) PID controller

(b) FOPID controller

(c) TID controller

(d) The proposed LFC based on the hybrid controller

FIGURE 3. The block diagram of existing FO and the proposed LFC hybrid controller.

C. THE PROPOSED FREQUENCY REGULATION CONTROLLER

The proposed frequency regulation method is based on employing hybrid FO controller for the LFC in coordination with FOPID controller for the SMES system. The determination of the optimized controller parameters for both controllers in the two-area can effectively enhance the frequency regulation of the system. The proposed LFC controller is based on the hybrid FO controller, which combines the features of the FOPID controller with the TID controller. The proposed LFC hybrid controller combines the FO integral

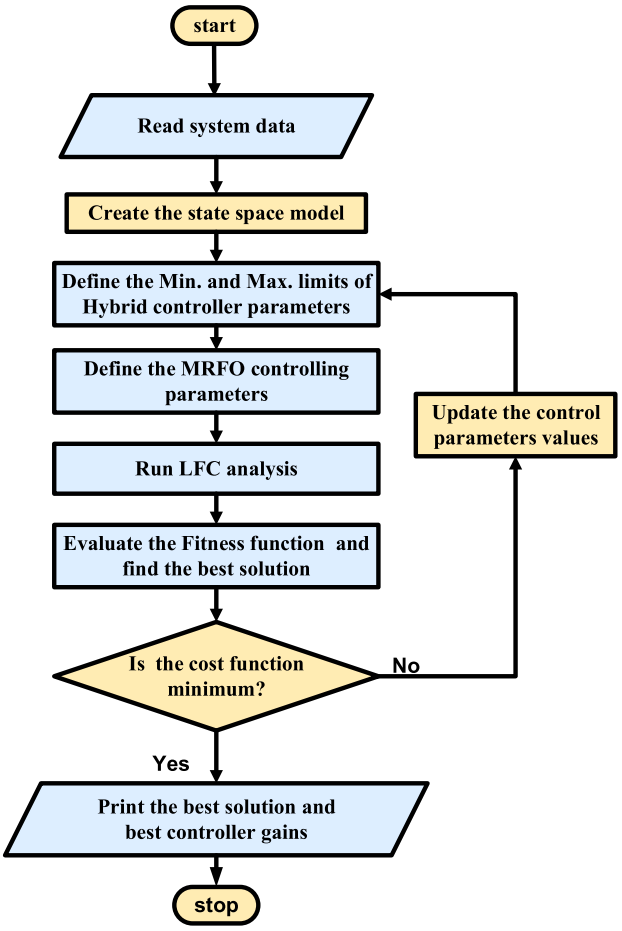

FIGURE 4. The procedures for determining the optimal controller parameters in the proposed MRFO method.

and derivative terms from the FOPID controller with the TID controller. The FO integral and derivative terms result in improving the system stability in addition to its robustness. Moreover, the two terms are advantageous at reducing the settling time of the controller during disturbances. Adding the FO derivative and integral terms would result in enriching the TID controller with more degree-of-freedom than its integer integral and derivative terms. Therefore, a hybrid controller is proposed in order to benefit from the features of the TID and FOPID controllers. The mathematical representation of the proposed LFC method based on the hybrid controller is represented as follows:

$$C(s) = \frac{Y(s)}{E(s)} = K_t \; s^{-(\frac{1}{n})} + \frac{K_i}{s^{\lambda}} + K_d \; s^{\mu} \tag{23}$$

Fig. 3d shows the block diagram of the hybrid TID-FOPID controller. It can be seen that there are six different tunable parameters in the hybrid controller. Proper tuning process is required for the controller parameters to optimize the system performance. The recent advanced optimization methods are employed for simultaneously determining the optimal parameters of frequency regulation controllers. In the following sections, the designed objective function and the proposed optimization method are introduced for both the SMES and LFC controllers in the two-area system.

IV. THE PROPOSED OPTIMIZATION METHOD

A. THE OPTIMIZATION PROBLEM

The design process of the various controllers in the interconnected power systems faces several challenges of the future high penetration levels of RESs and system uncertainties that increase the multi-area frequency deviations and tie-line power flow fluctuations. In order to effectively damp out these fluctuations and to enhance the system performance, the hybrid controller is proposed in this paper as a secondary controller for areas a and area b. In addition, the FOPID is used as a controller for ($SMES_a$) and ($SMES_b$) devices to accurately monitor the system load variations and promote the operation of the thermal and hydraulic generating units as shown in Fig.2. The frequency deviations of area a (Δf_a) and area b (Δf_b) represent the input signals to these controllers. Thus, there are two different controllers in each area to assure a more secure operation for the interconnected power system with considering the high penetration of the RESs. This in turn shows that there are more than 20 parameters of the hybrid controller in the LFC loop and the SMES controller, which need to be precisely selected. Therefore, this study employs the recently developed MRFO algorithm to optimally tune the SMES controller parameters ($k_{pi} - k_{Ii} - k_{di} - \mu - \lambda$), and the LFC parameters ($k_{ti} - k_{Ii} - k_{pi} - n$) in each area. Moreover, the issue of utilizing a hybrid HVAC/HVDC tie-line is also considered in the proposed multi-area system. Fig. 4 illustrates the procedures for determining the optimal parameters using the MRFO method. To properly enhance the power system performance, a proper selection of the objective cost function is required to maintain the system dynamics. There are many classical cost functions, which have been used in the literature such as integral squared error (ISE), integral time squared error (ITSE), integral-absolute error (IAE), the integral time absolute error (ITAE), etc [44]. In this paper, the ISE is selected as a single objective function to determine the optimum parameters of the proposed controllers. The ISE represents the most widely adopted cost function in literature due to its simplicity in calculation [45]. Moreover, the ISE criteria provides minimum overshoot and shows a fast response in comparison to the other integral errors due to the use of larger square values to eliminate negative error components. In addition, large errors can be penalized compared to smaller ones by using the ISE objective function. Therefore, the ISE criteria is utilized to optimize the parameters of the proposed controllers as:

$$\begin{aligned} CostFunction &= minimize(ISE) = J_{min} \\ &= \int_0^{t_s} \{(\Delta f_a)^2 + (\Delta f_b)^2 + (\Delta P_{tie,eq})^2\} \end{aligned} \tag{24}$$

where, T is the range of simulation time, Δf_a is the frequency change in area a, Δf_b is the frequency change in area b, and $\Delta P_{tie,eq}$ is the power change in tie-line connecting areas

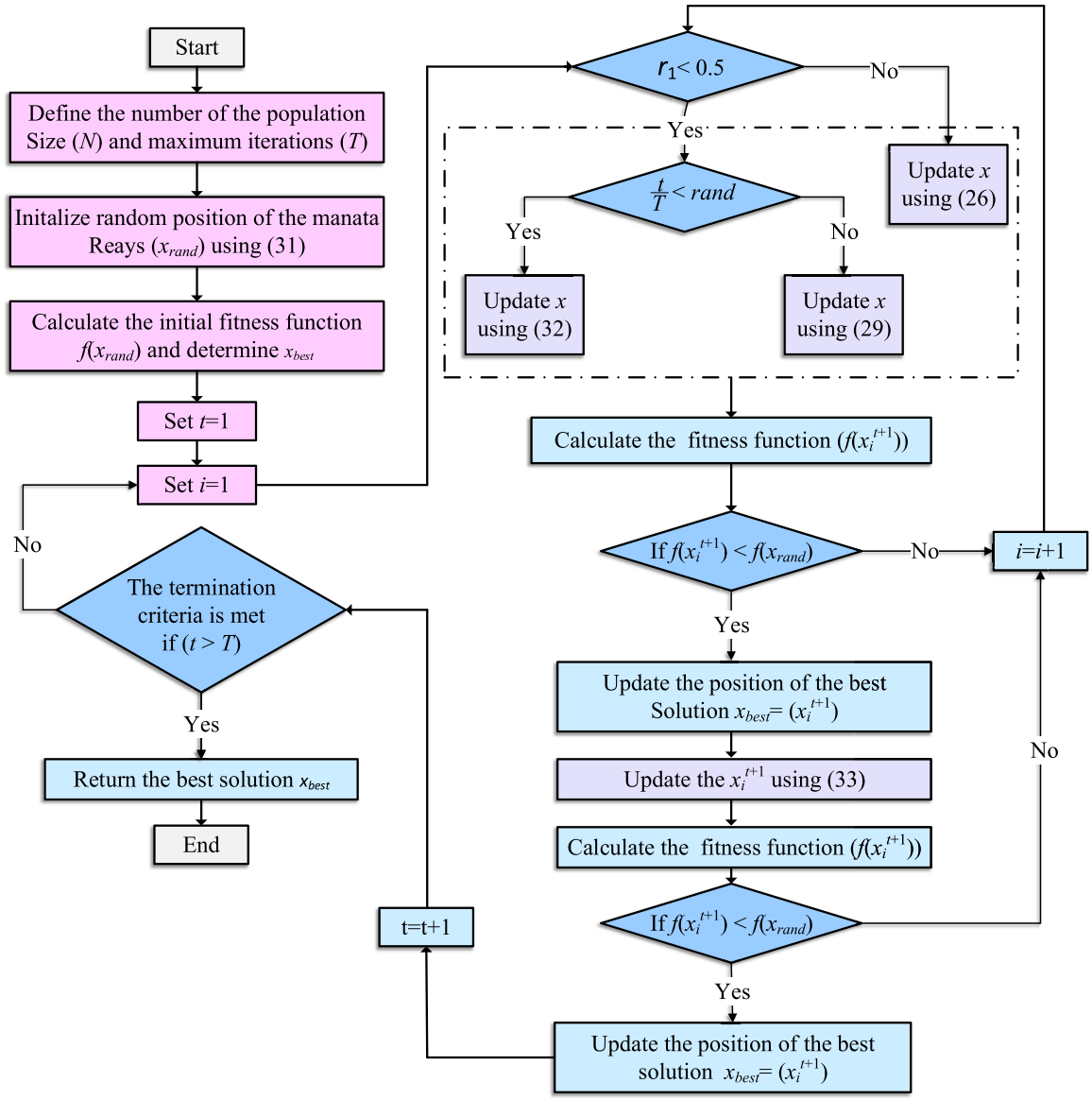

FIGURE 5. The flowchart of the MRFO method for minimizing the objective function.

a and b. To minimize the cost function J, the proposed controllers' parameters are subjected to the following constraints:

$$\begin{aligned} K_p^{min} &\le K_p \le K_p^{max} \\ K_i^{min} &\le K_i \le K_i^{max} \\ K_d^{min} &\le K_d \le K_d^{max} \\ K_t^{min} &\le K_t \le K_t^{max} \\ 0 &\le \lambda, \quad \mu \le 1 \\ 2 &\le n \le 10 \end{aligned} \tag{25}$$

where, the minimum and maximum limits of the proportional, integral, derivative and tilt gains are selected in the proposed method in the range of [0, 10], respectively.

B. THE MANTA RAY FORAGING OPTIMIZATION ALGORITHM (MRFO)

A metaheuristic optimization method has been presented based on the manta ray foraging optimizer (MRFO), which is inspired by the foraging strategy and followed by the manta rays within catching their preys [37]. This optimization method has three main foraging operators; namely, chain, cyclone and the somersault foraging. During the chain foraging stage, the manta rays takes into consideration the high concentration plankton represents the desired objective (the best targeted solution) [46]. Thence, they are lined up to form the foraging chain. Wherein, every individual moves towards the food and manta rays in its front, the update process for each individual is achieved by the obtaining best solution during each iteration, and obtaining the solution for the one that

is in front of current individual. In MRFO method, the chain foraging process is mathematically modelled as follows [47]:

$$x_i^{t+1} = \begin{cases} x_i^t + r.(x_{best}^t - x_i^t) + \alpha(x_{best}^t - x_i^t), & i = 1 \\ x_i^t + r.(x_{i-1}^t - x_i^t) + \alpha(x_{best}^t - x_i^t), & i = 2:N \end{cases} \quad (26)$$

where, x_i^t represents the i^{th} individual position for the iteration t; r denotes to random vector; x_{best}^t represents the best solution for the t^{th} iteration, N represents the manta rays number, and α denotes to the weighting coefficient, which can be determined as following:

$$\alpha = 2 \times r \times \sqrt{|\log(r)|} \quad (27)$$

Based on (26), the position is estimated for the all the i^{th} individuals, except the first individual, with the position of both the $(i-1)^{th}$ individual and the best individual x_{best}^t. After the manta rays determine the position of plankton patch, they are combined to from the chain and they swim towards prey in spiral shape. Besides, individuals swim towards their front side manta ray, which is followed by cyclone foraging stage. The above-mentioned movements can be mathematically formulated as follows [47]:

$$\begin{aligned} x_i^{t+1} &= x_{best} + r.(x_{i-1}^t - x_i^t) + e^{b\omega}.\cos(2\pi\omega).(x_{best} - x_i^t) \\ y_i^{t+1} &= y_{best} + r.(y_{i-1}^t - y_i^t) + e^{b\omega}.\cos(2\pi\omega).(y_{best} - y_i^t) \end{aligned} \quad (28)$$

where, ω represents random number. Whereas, the stage of cyclone foraging is represented as following:

$$x_i^{t+1} = \begin{cases} x_{best} + r.(x_{best}^t - x_i^t) + \beta(x_{best}^t - x_i^t), & i = 1 \\ x_{best} + r.(x_{i-1}^t - x_i^t) + \beta(x_{best}^t - x_i^t), & i = 2:N \end{cases} \quad (29)$$

where, β denotes to weighting factor, which can be determined as following:

$$\beta = 2e^{r_1}\left(\frac{T - t + 1}{T}\right).\sin(2\pi r_1) \quad (30)$$

where, t represents the current iteration, T denotes to maximum number of the iterations, and r_1 is a random number. Improved exploitation can be achieved by cyclone foraging stage for determining best region of the solution due to that all the existing manta rays contribute in the food searching process according to their reference position. In addition, another enhancement of the exploitation processes can be obtained in this process by forcing individuals to the search process for new positions that are located far away from the current best position. Performing this action can be made through the assignment of a random position within the searching space as following [46]:

$$x_{rand} = Lb + r.(Ub - Lb) \quad (31)$$

$$x_i^{t+1} = \begin{cases} x_{rand} + r.(x_{rand}^t - x_i^t) + \beta(x_{rand}^t - x_i^t), & i = 1 \\ x_{rand} + r.(x_{i-1}^t - x_i^t) + \beta(x_{rand}^t - x_i^t), & i = 2:N \end{cases} \quad (32)$$

where, Ub and Lb represent upper and lower limits for the variables of the problem, x_{rand} denotes to random position that is assigned for searching space. The last stage in the MRFO method is the somersault foraging, wherein food is recognized as hinge. During this stage, each of the manta rays tends to perform swimming backward and forward around the food hinge, and then tumbling to the new position. The mathematical expression of this process can be performed as following [47]:

$$x_i^{t+1} = x_i^t + S.(r_2. - r_3.x_i^t), \quad i = 1, 2, \ldots, N \quad (33)$$

where, S represents the somersault factor that is employed for deciding the somersault range of manta rays, and r_2 and r_3 represent random numbers. By referring to (28), individuals can move towards any position within searching space between the current position and the symmetrical position around the food hinge. The conversion process to optimal solution is achieved through reducing the distance among the position of manta rays and the best position. Therefore, the range of somersault foraging is reduced in adaptive manner during iterations. Fig. 5 summarizes the followed steps in the MRFO method for the minimization process.

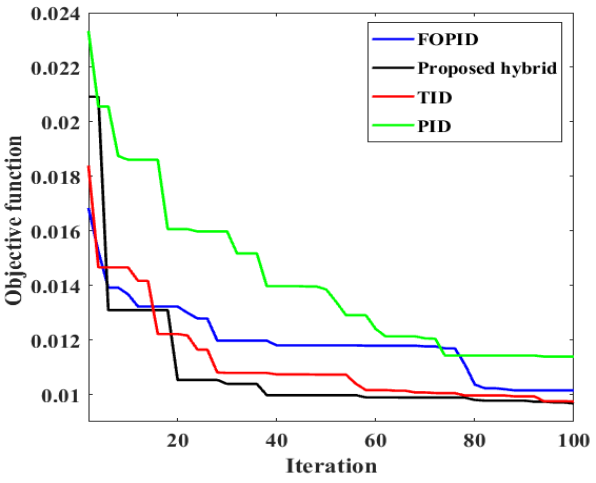

FIGURE 6. Convergence curve at scenario 1.

V. SIMULATION RESULTS

A. SCENARIO 1: LOAD STEP CHANGE

The first scenario is conducted to evaluate the performance of the proposed hybrid controller for the studied multi-area power system using the controller parameters listed in Table. 2. A 10% step load change at the time 15 s is applied to area a without the presence of any RESs in both areas. The convergence curve of the objective function (ISE) based on MRFO is shown in Fig. 6. The results of frequency deviation in both areas a, b are shown in Fig. 7a and Fig. 7b, respectively. As shown in these figures, the frequency deviation curve varies considerably while the PID controller is used. Although The PID damps out system oscillations, however, it cannot restore the steady state frequency to its original value. Moreover, the TID and FOPID controllers damp out the frequency fluctuations of area a within about 40 s to 50 s time period with relatively high overshoot and undershoot.

TABLE 2. Optimal coefficients of the controllers by using MRFO.

Controller	Type	Coefficients					
		K_p	K_i	K_d	K_t	λ	μ
LFC	PID_a	1.9647	1.871	1.5242	-	-	-
	PID_b	1.141	0.4278	0.8725	-	-	-
	TID_a	-	1.8869	1.4336	1.9384	1	1
	TID_b	-	0.7102	1.6396	1.509	1	1
	$FOPID_a$	1.8445	1.988	1.4823	-	0.92	0.51
	$FOPID_b$	1.4099	0.0522	0.37968	-	0.94	0.7
	Proposed hybrid (area a)	-	1.9935	1.606	1.9376	0.43	0.28
	Proposed hybrid (area b)	-	0.87343	0.27152	1.5926	0.35	0.18
SMES controller	$SMES_a$	1.6079	0.8966	1.7861	-	1	1
	$SMES_b$	0.8765	0.7709	1.4275	-	1	1

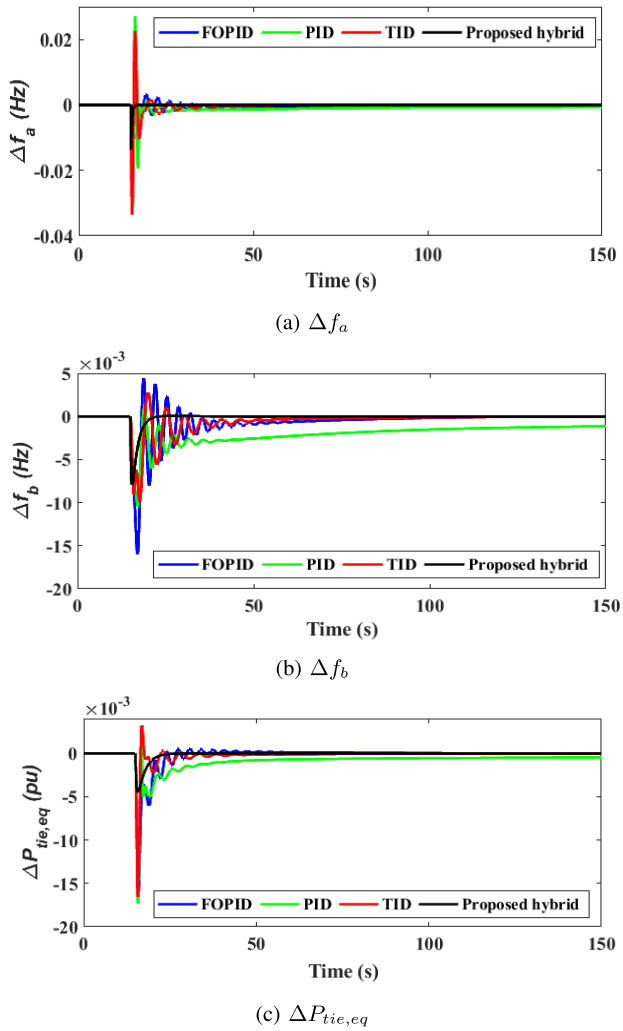

FIGURE 7. System response with the optimized controllers at scenario 1.

Whereas, the proposed hybrid controller alleviates the frequency oscillations within about 18 s, which is being a shorter period compared to the previous ones. Furthermore, the proposed hybrid controller has the lowest oscillation of tie-line power compared to other controllers as shown in Fig. 7b. From the results, it is clear that the hybrid controller exhibits more satisfactory performance than PID, TID, and FOPID controllers in terms of ISE, settling time, and overshoot.

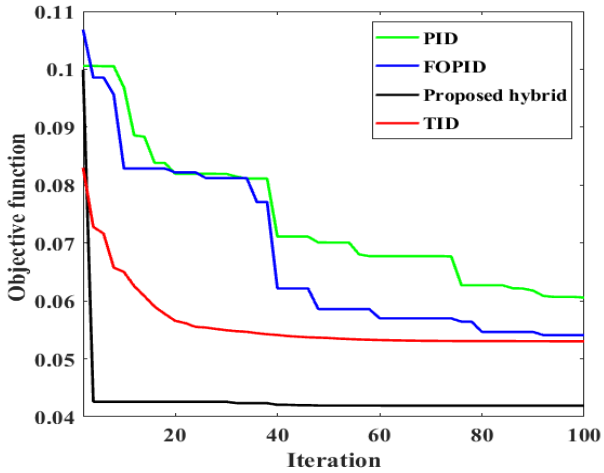

FIGURE 8. Convergence curve at scenario 2.

B. SCENARIO 2: IMPACT OF RESs FLUCTUATIONS

In addition to the load disturbance, the RESs nature fluctuations can possess detrimental influences on the frequency response of power system due to the existing inverter-based structures in power microgrid systems and the absence of rotational masses, as well. Therefore, a pattern of wind speed fluctuation is added to the studied system at time 100 s beside PV integration from the starting time of simulation in addition to a 10% step load disturbance at 15 s. The convergence curve of the objective function based on MRFO and the performance of the suggested controllers are shown in Fig. 8 and Fig. 9, respectively. Although the PID controller can suppress the high overshoot and undershoot of the frequency deviations, it cannot restore them to an acceptable value as shown in Fig. 9b, and Fig. 9c. However, the TID and FOPID controllers give satisfactory results compared to the PID with the reasonable capability to damp out the frequency and tie-line power oscillations as seen in Fig. 9b, Fig. 9c, and Fig. 9d. On the other hand, the cooperative action of the proposed hybrid controller with the SMES based-FOPID controller confirms their robustness compared to other control methods as can be observed from Fig. 9. The proposed controller achieves a settling time of 21 s compared to 35 s and 39 s for the TID and FOPID controllers, respectively.

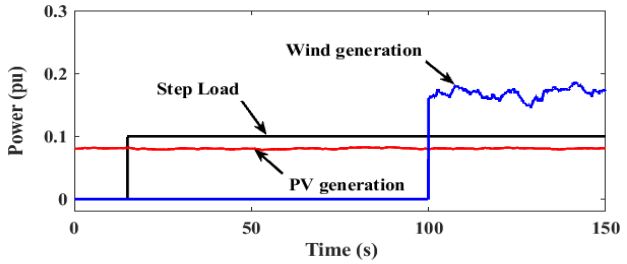

(a) The generation and load waveforms

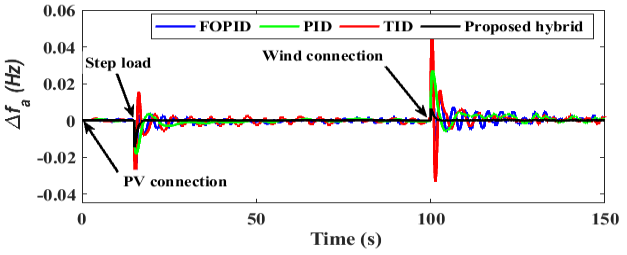

(b) Δf_a

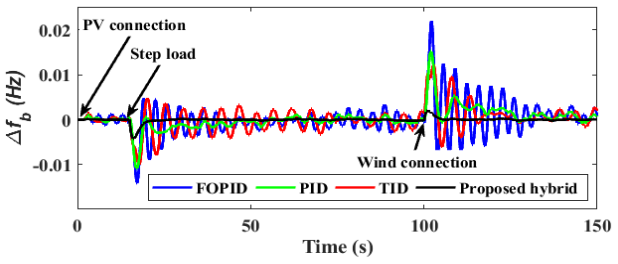

(c) Δf_b

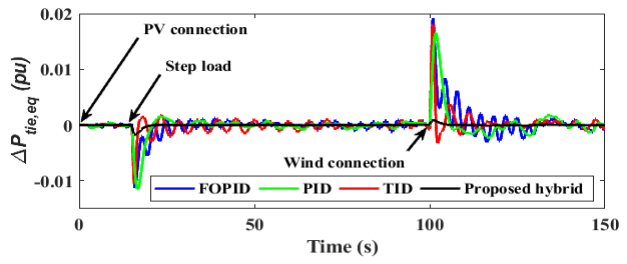

(d) $\Delta P_{tie,eq}$

FIGURE 9. System response with the optimized controllers at scenario 2.

C. SCENARIO 3: MULTI-LOAD DISTURBANCES

In this scenario, the power system under study is subjected to three disturbance stages of load changes at 20 s, 60 s, 110 s, respectively as seen in Fig. 10a. The obtained results under this case for both areas frequencies and tie-line power deviations are shown in Fig. 10. It can be observed that the system fluctuations are increased and the frequency error of the two-area cannot be restored to its zero value by using only the PID controller in the LFC loop. Whereas, the TID and FOPID can damp out the peak deviation of frequency and tie-line power but with a long time to be settled. The proposed hybrid cooperative controller exhibits better dynamic performance to damp out the frequency and power oscillations in comparison to FOPID, TID, and PID controllers. The proposed coordination among the LFC controller and SMES controller represents the best combination compared to the other controllers.

D. SCENARIO 4: ROBUSTNESS ANALYSIS

In order to investigate the performance of the proposed hybrid controller, the studied system is subjected to severe disturbances, including load disturbances, wind power fluctuations, and physical parameter variations, which can lead to system instability. The power system parameters are varied in this scenario as follows: $H = -30\%$; $D = +20\%$; $T_g = +30\%$; $T_t = -25\%$; $T_{SMES} = +35\%$ under the same operating conditions of RESs and load fluctuations of the earlier scenario 2. As can be seen in Fig. 12, the PID controller with the energy storage system based-FOPID controller cannot diminish the frequency oscillations and tie-line power deviations during these severe changes. Furthermore, the TID and FOPID controllers based on the MRFO have failed in damping out the high overshoots and undershoots, especially at the instant of wind generation connection at time 100 s. However, they can restore the original frequency and power values after a long settling time. In contrast, by employing the proposed MRFO-based hybrid controller coordinated with the SMES-FOPID controller, the amplitude of the system fluctuations becomes nearly zero with fast settling time as shown in Table 3. Moreover, a faster and linear convergence curve is achieved compared to the other studied controllers, as clarified in Fig. 11. Hence, it can be concluded that the coordination between the proposed hybrid FO controller in the LFC loop and SMES FOPID controller reduces the high system fluctuations and the system becomes more stable than using individual PID, TID, or FOPID controllers.

E. SCENARIO 5: MISSING THE HVDC LINK

In this scenario, the performance of the studied system is tested under the same extreme disturbances conditions of the previous scenario 4 of high wind power penetration, step loading, and parameters variations. In addition to these contingencies, the case study is subjected to a case of missing the HVDC link, which may lead to more fluctuations in the system frequency and tie-line power. The proposed method based on the SMES device and optimal hybrid LFC provides powerful performance due to its better fluctuations damping property in addition to the mitigation of the frequency and tie-power deviations than the other controllers as shown in Fig. 13. It can be also seen that the PID cannot withstand this scenario due to the high failure rates of the power electronic-based HVDC tie-line. Moreover, the TID and FOPID based controllers exhibit poor damping characteristics. However, the proposed hybrid controller settles the oscillations to zero very fast and produces significant reductions in their peak value as summarized in Table. 3. However, this scenario clarifies the importance of utilizing the HVDC link compared with the previous case, which has an improvement in minimizing the peak overshoot and damping oscillations with a fast-settled response.

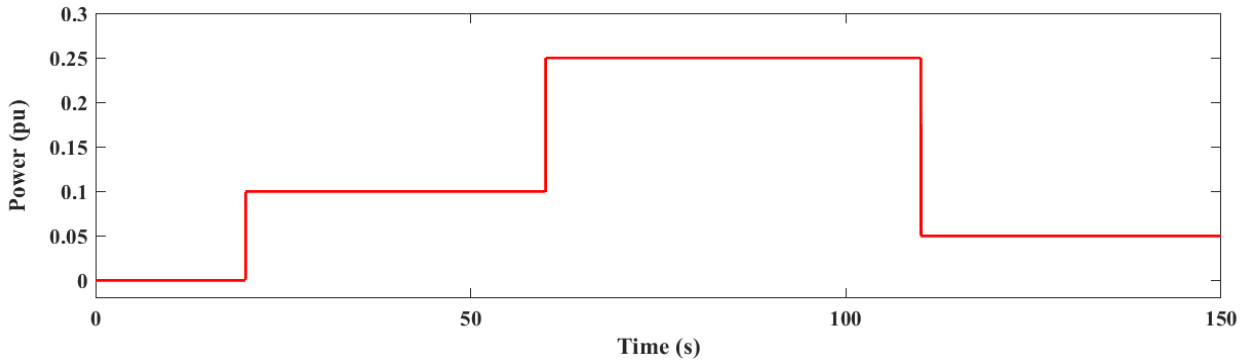

(a) The generation and load waveforms

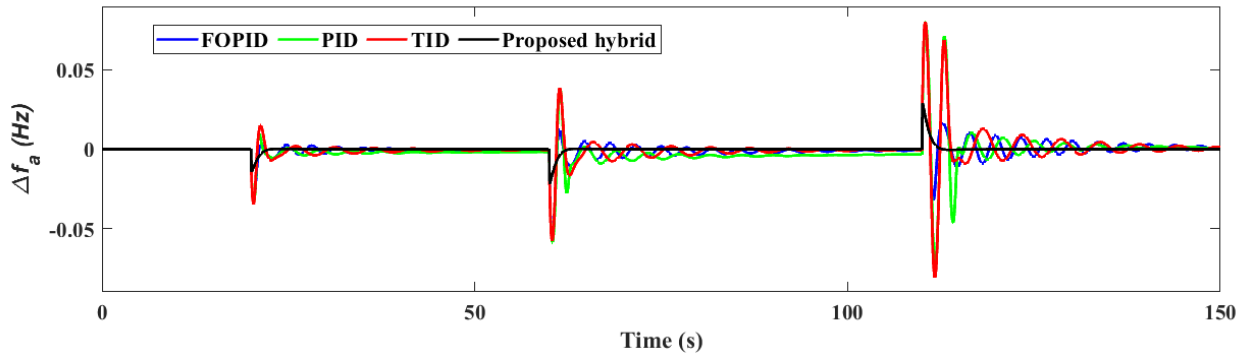

(b) Δf_a

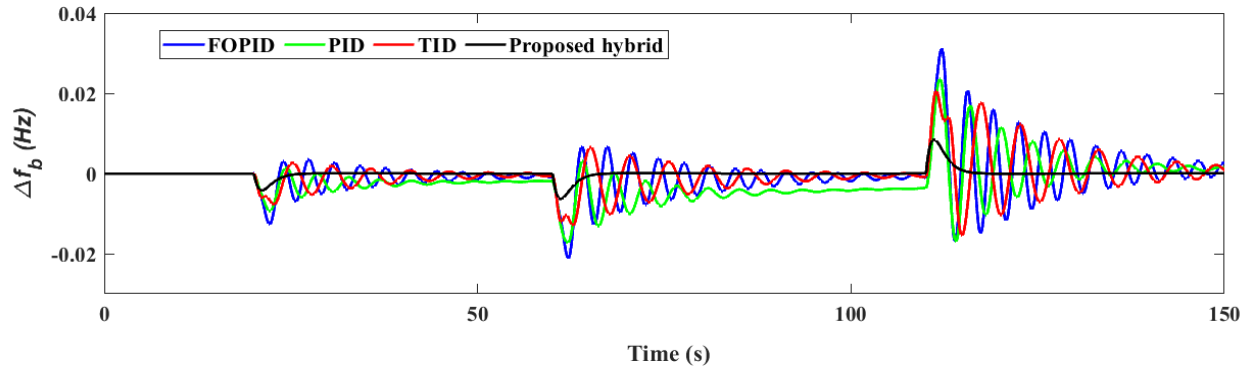

(c) Δf_b

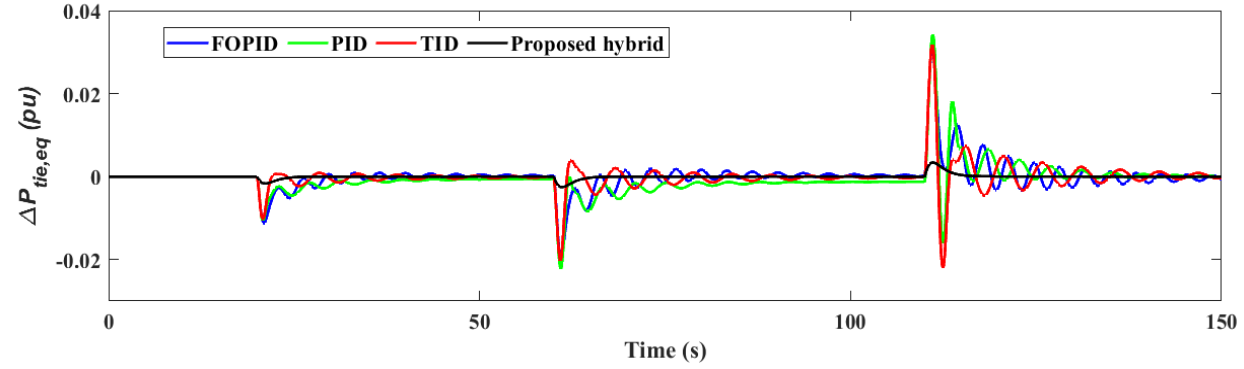

(d) $\Delta P_{tie,eq}$

FIGURE 10. System response with the optimized controllers at scenario 3.

TABLE 3. Estimated maximum overshoot (MO) and settling time (ST) for the studied scenarios (at 15 s).

Scenario	Algorithm	Δf_a		Δf_b		$\Delta P_{tie,eq}$	
		MO	ST (s)	MO	ST (s)	MO	ST (s)
Scenario 1	PID	0.0331	-	0.0105	-	0.0173	-
	FOPID	0.0326	50	0.016	84	0.0169	109
	TID	0.0335	40	0.0098	79	0.0166	101
	Proposed hybrid	0.0135	18	0.0078	23	0.0045	30
Scenario 2	PID	0.0182	79	0.0108	57	0.0115	49
	FOPID	0.0336	51	0.0141	-	0.0113	-
	TID	0.0343	39	0.0110	-	0.0105	-
	Proposed hybrid	0.0144	21	0.0042	27	0.0017	22
Scenario 3	PID	0.0343	-	0.0094	-	0.0107	-
	FOPID	0.0333	51	0.0126	-	0.0112	-
	TID	0.0341	43	0.0077	-	0.0103	-
	Proposed hybrid	0.0144	22	0.0042	28	0.0017	29
Scenario 4	PID	0.0323	-	0.0082	-	0.0094	-
	FOPID	0.0322	75	0.0111	97	0.0103	99
	TID	0.0329	70	0.0059	91	0.0092	94
	Proposed hybrid	0.0144	21	0.0041	23	0.0016	25
Scenario 5	PID	0.0324	-	0.0078	-	0.0085	-
	FOPID	0.0322	79	0.0104	98	0.0095	82
	TID	0.0329	71	0.0057	93	0.0083	76
	Proposed hybrid	0.0184	26	0.0060	20	0.0024	22

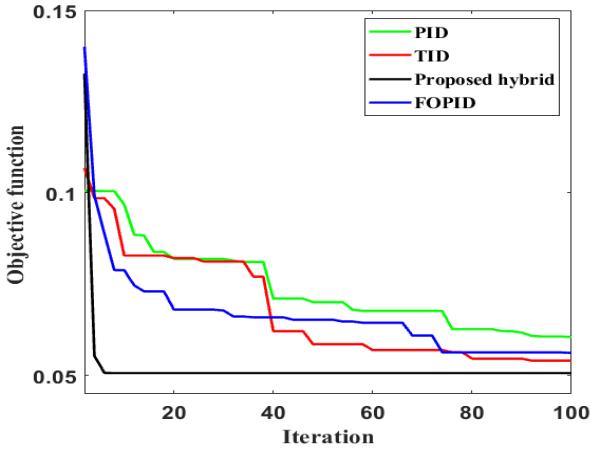

FIGURE 11. Convergence curve at scenario 4.

VI. PERFORMANCE COMPARISONS AND DISCUSSIONS

Table. 3 illustrates a detailed comparison between the proposed cooperative hybrid controller with other addressed controllers in the context. The table compares the values of the overshoot and settling time of the dynamic performance of the frequency deviations and tie-line power in each scenario. It can be seen in all scenarios that the proposed controller improves the dynamic response of the frequency deviation and the tie-line power and brings them to zero in the steady state. The proposed cooperative hybrid controller achieves the minimum overshoots and settling times in all scenarios. The overshoot in frequency deviations and tie-line powers are decreased to more than 40% of that one's using PID, FOPID, or TID. Moreover, the settling time has been decreased to more than 50% of the other controllers. Even in severe scenarios and system uncertainties, the proposed cooperative controller has the capability to properly damping any fluctuations in the frequency or the tie-line power. Therefore, the table shows the superiority of the proposed cooperative hybrid controller over the existing controllers for achieving an improved dynamic response, mitigating the deviations of area

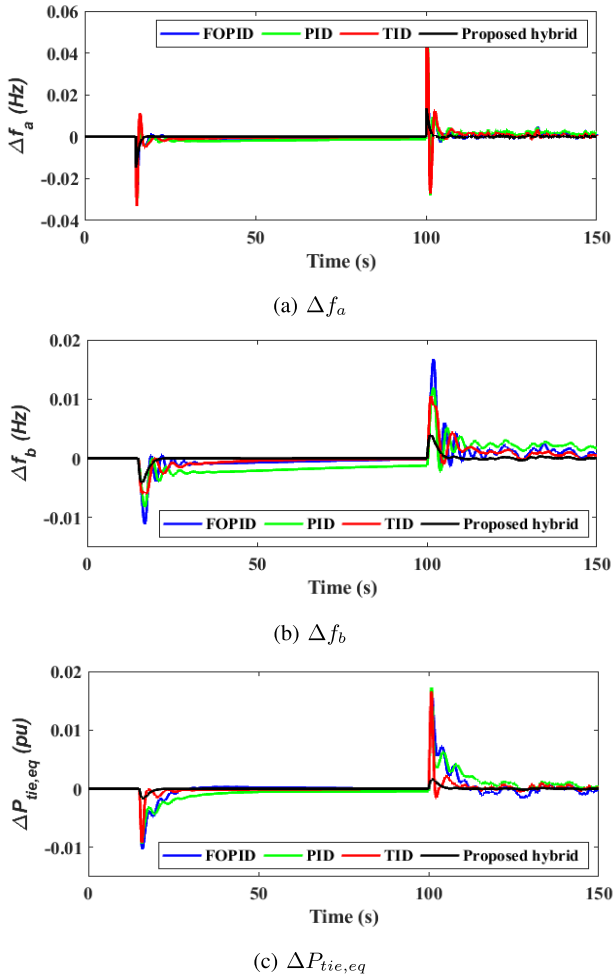

FIGURE 12. System response with the optimized controllers under physical parameters variations for the sensitivity analysis at scenario 4.

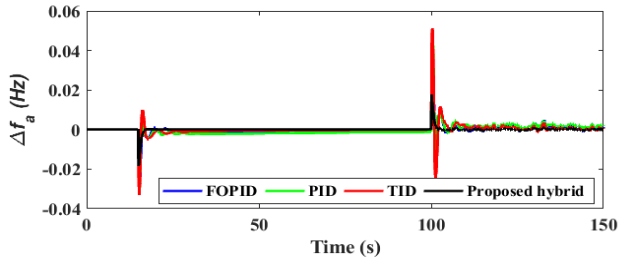

(a) Δf_a

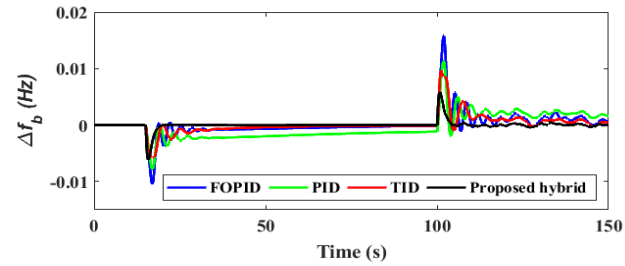

(b) Δf_b

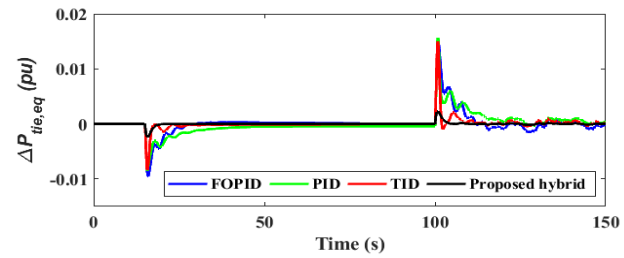

(c) $\Delta P_{tie,eq}$

FIGURE 13. System response with disconnection of HVDC tie-line under the optimized controllers at scenario 5.

frequency and tie-line power, and maintaining stable operation at various system disturbances, generation uncertainty, and system parameters variations.

VII. CONCLUSION

This paper proposes a cooperative control scheme of a hybrid fractional order controller in the LFC loop and SMES technology to enhance the stability of interconnected power systems. This coordinated control scheme is designed based on the MRFO algorithm as an effective optimization technique, which is employed to optimize the parameters of the hybrid LFC and SMES FOPID controllers. The simulated results show that the cooperative hybrid controller based on the developed MRFO outperforms the other controllers, such as PID, TID, and FOPID. It is the most effective in regulating the frequency and tie-line power oscillations due to the high fluctuations of RESs and multi-load changes. The proposed method provides superior performance at achieving a reduction in the overshoot in frequency deviations and tie-line power to more than 40% compared to PID, FOPID, or TID controllers. In addition, the settling time is reduced by the proposed method to more than 50% compared to the other controllers. Moreover, it provides high robustness against the variation of power system physical parameters. Furthermore, the coordinated hybrid LFC with SMES controller possesses superior robustness in case of HVDC tie-line fault and against the system parameters uncertainty. On the other hand, the presented MRFO algorithm has improved the learning ability and the inter-generational information transmission, wherein they are integrated into sequential balanced phases to control the exploration-exploitation problem. Hence, it can be applied to solve many engineering problems.

REFERENCES

[1] S. M. Said, M. Aly, and H. Balint, "An efficient reactive power dispatch method for hybrid photovoltaic and superconducting magnetic energy storage inverters in utility grids," *IEEE Access*, vol. 8, pp. 183708–183721, 2020.

[2] S. K. Pandey, S. R. Mohanty, and N. Kishor, "A literature survey on load–frequency control for conventional and distribution generation power systems," *Renew. Sustain. Energy Rev.*, vol. 25, pp. 318–334, Sep. 2013.

[3] P. C. Pradhan, R. K. Sahu, and S. Panda, "Firefly algorithm optimized fuzzy PID controller for AGC of multi-area multi-source power systems with UPFC and SMES," *Eng. Sci. Technol., Int. J.*, vol. 19, no. 1, pp. 338–354, Mar. 2016.

[4] E. Rakhshani, P. Rodriguez, A. Mir Cantarellas, and D. Remon, "Analysis of derivative control based virtual inertia in multi-area high-voltage direct current interconnected power systems," *IET Gener., Transmiss. Distribution*, vol. 10, no. 6, pp. 1458–1469, Apr. 2016.

[5] T. Kerdphol, F. S. Rahman, Y. Mitani, M. Watanabe, and S. Kufeoglu, "Robust virtual inertia control of an islanded microgrid considering high penetration of renewable energy," *IEEE Access*, vol. 6, pp. 625–636, 2018.

[6] S. Saxena and Y. V. Hote, "Load frequency control in power systems via internal model control scheme and model-order reduction," *IEEE Trans. Power Syst.*, vol. 28, no. 3, pp. 2749–2757, Aug. 2013.

[7] X. Lv, Y. Sun, Y. Wang, and V. Dinavahi, "Adaptive event-triggered load frequency control of multi-area power systems under networked environment via sliding mode control," *IEEE Access*, vol. 8, pp. 86585–86594, 2020.

[8] R. R. Shoults and J. A. Jativa Ibarra, "Multi-area adaptive LFC developed for a comprehensive AGC simulator," *IEEE Trans. Power Syst.*, vol. 8, no. 2, pp. 541–547, May 1993.

[9] İ. Kocaarslan and E. Çam, "Fuzzy logic controller in interconnected electrical power systems for load-frequency control," *Int. J. Electr. Power Energy Syst.*, vol. 27, no. 8, pp. 542–549, Oct. 2005.

[10] X. Yu and K. Tomsovic, "Application of linear matrix inequalities for load frequency control with communication delays," *IEEE Trans. Power Syst.*, vol. 19, no. 3, pp. 1508–1515, Aug. 2004.

[11] C. S. Rao, S. S. Nagaraju, and P. S. Raju, "Automatic generation control of TCPS based hydrothermal system under open market scenario: A fuzzy logic approach," *Int. J. Electr. Power Energy Syst.*, vol. 31, nos. 7–8, pp. 315–322, Sep. 2009.

[12] G. Ray, S. Dey, and T. K. Bhattacharyya, "Multi-area load frequency control of power systems: A decentralized variable structure approach," *Electr. Power Compon. Syst.*, vol. 33, no. 3, pp. 315–331, Dec. 2004.

[13] A. M. Ersdal, L. Imsland, and K. Uhlen, "Model predictive load-frequency control," *IEEE Trans. Power Syst.*, vol. 31, pp. 777–785, Jan. 2016.

[14] M. Shiroei and A. M. Ranjbar, "Supervisory predictive control of power system load frequency control," *Int. J. Electr. Power Energy Syst.*, vol. 61, pp. 70–80, Oct. 2014.

[15] Z. Yan and Y. Xu, "Data-driven load frequency control for stochastic power systems: A deep reinforcement learning method with continuous action search," *IEEE Trans. Power Syst.*, vol. 34, no. 2, pp. 1653–1656, Mar. 2019.

[16] Z. Yan and Y. Xu, "A multi-agent deep reinforcement learning method for cooperative load frequency control of a multi-area power system," *IEEE Trans. Power Syst.*, vol. 35, no. 6, pp. 4599–4608, Nov. 2020.

[17] Z. Yan and Y. Xu, "Real-time optimal power flow: A lagrangian based deep reinforcement learning approach," *IEEE Trans. Power Syst.*, vol. 35, no. 4, pp. 3270–3273, Jul. 2020.

[18] S. Panda, B. Mohanty, and P. K. Hota, "Hybrid BFOA–PSO algorithm for automatic generation control of linear and nonlinear interconnected power systems," *Appl. Soft Comput.*, vol. 13, no. 12, pp. 4718–4730, Dec. 2013.

[19] C. K. Shiva, G. Shankar, and V. Mukherjee, "Automatic generation control of power system using a novel quasi-oppositional harmony search algorithm," *Int. J. Electr. Power Energy Syst.*, vol. 73, pp. 787–804, Dec. 2015.
[20] B. Mohanty, S. Panda, and P. K. Hota, "Controller parameters tuning of differential evolution algorithm and its application to load frequency control of multi-source power system," *Int. J. Electr. Power Energy Syst.*, vol. 54, pp. 77–85, Jan. 2014.
[21] R. K. Sahu, S. Panda, U. K. Rout, and D. K. Sahoo, "Teaching learning based optimization algorithm for automatic generation control of power system using 2-DOF PID controller," *Int. J. Electr. Power Energy Syst.*, vol. 77, pp. 287–301, May 2016.
[22] P. Dash, L. Saikia, and N. Sinha, "Automatic generation control of multi area thermal system using bat algorithm optimized PD–PID cascade controller," *Int. J. Electr. Power Energy Syst.*, vol. 68, pp. 364–372, Jun. 2015.
[23] M. Raju, L. C. Saikia, and N. Sinha, "Automatic generation control of a multi-area system using ant lion optimizer algorithm based PID plus second order derivative controller," *Int. J. Electr. Power Energy Syst.*, vol. 80, pp. 52–63, Sep. 2016.
[24] M. Gheisarnejad, "An effective hybrid harmony search and cuckoo optimization algorithm based fuzzy PID controller for load frequency control," *Appl. Soft Comput.*, vol. 65, pp. 121–138, Apr. 2018.
[25] S. Prakash and S. K. Sinha, "Simulation based neuro-fuzzy hybrid intelligent PI control approach in four-area load frequency control of interconnected power system," *Appl. Soft Comput.*, vol. 23, pp. 152–164, Oct. 2014.
[26] C. Huang, J. Li, S. Mu, and H. Yan, "Linear active disturbance rejection control approach for load frequency control of two-area interconnected power system," *Trans. Inst. Meas. Control*, vol. 41, no. 6, pp. 1562–1570, Apr. 2019.
[27] S. Oshnoei, A. Oshnoei, A. Mosallanejad, and F. Haghjoo, "Contribution of GCSC to regulate the frequency in multi-area power systems considering time delays: A new control outline based on fractional order controllers," *Int. J. Electr. Power Energy Syst.*, vol. 123, Dec. 2020, Art. no. 106197.
[28] R. Kumar Sahu, S. Panda, A. Biswal, and G. T. Chandra Sekhar, "Design and analysis of tilt integral derivative controller with filter for load frequency control of multi-area interconnected power systems," *ISA Trans.*, vol. 61, pp. 251–264, Mar. 2016.
[29] A. Delassi, S. Arif, and L. Mokrani, "Load frequency control problem in interconnected power systems using robust fractional PIλd controller," *Ain Shams Eng. J.*, vol. 9, no. 1, pp. 77–88, Mar. 2018.
[30] Y. Arya, "A new optimized fuzzy FOPI-FOPD controller for automatic generation control of electric power systems," *J. Franklin Inst.*, vol. 356, no. 11, pp. 5611–5629, Jul. 2019.
[31] M. Gheisarnejad and M. H. Khooban, "Design an optimal fuzzy fractional proportional integral derivative controller with derivative filter for load frequency control in power systems," *Trans. Inst. Meas. Control*, vol. 41, no. 9, pp. 2563–2581, Jan. 2019.
[32] Y. Arya, "Improvement in automatic generation control of two-area electric power systems via a new fuzzy aided optimal PIDN-FOI controller," *ISA Trans.*, vol. 80, pp. 475–490, Sep. 2018.
[33] S. P. Ghoshal and S. K. Goswami, "Application of GA based optimal integral gains in fuzzy based active power-frequency control of non-reheat and reheat thermal generating systems," *Electr. Power Syst. Res.*, vol. 67, no. 2, pp. 79–88, Nov. 2003.
[34] T. K. Mohapatra and B. K. Sahu, "Design and implementation of SSA based fractional order PID controller for automatic generation control of a multi-area, multi-source interconnected power system," in *Proc. Technol. Smart-City Energy Secur. Power (ICSESP)*, Mar. 2018, pp. 1–6.
[35] S. M. Abd-Elazim and E. S. Ali, "Load frequency controller design of a two-area system composing of PV grid and thermal generator via firefly algorithm," *Neural Comput. Appl.*, vol. 30, no. 2, pp. 607–616, Jul. 2018.
[36] S. A. Taher, M. H. Fini, and S. F. Aliabadi, "Fractional order PID controller design for LFC in electric power systems using imperialist competitive algorithm," *Ain Shams Eng. J.*, vol. 5, no. 1, pp. 121–135, Mar. 2014.
[37] W. Zhao, Z. Zhang, and L. Wang, "Manta ray foraging optimization: An effective bio-inspired optimizer for engineering applications," *Eng. Appl. Artif. Intell.*, vol. 87, Jan. 2020, Art. no. 103300.
[38] R. J. Abraham, D. Das, and A. Patra, "Automatic generation control of an interconnected hydrothermal power system considering superconducting magnetic energy storage," *Int. J. Electr. Power Energy Syst.*, vol. 29, no. 8, pp. 571–579, Oct. 2007.
[39] T. Kerdphol, M. Watanabe, Y. Mitani, and V. Phunpeng, "Applying virtual inertia control topology to SMES system for frequency stability improvement of low-inertia microgrids driven by high renewables," *Energies*, vol. 12, no. 20, p. 3902, Oct. 2019.
[40] A. Zamani, S. M. Barakati, and S. Yousofi-Darmian, "Design of a fractional order PID controller using GBMO algorithm for load–frequency control with governor saturation consideration," *ISA Trans.*, vol. 64, pp. 56–66, Sep. 2016.
[41] I. Pan and S. Das, "Fractional-order load-frequency control of interconnected power systems using chaotic multi-objective optimization," *Appl. Soft Comput.*, vol. 29, pp. 328–344, Apr. 2015.
[42] J. Morsali, K. Zare, and M. Tarafdar Hagh, "Applying fractional order PID to design TCSC-based damping controller in coordination with automatic generation control of interconnected multi-source power system," *Eng. Sci. Technol., Int. J.*, vol. 20, no. 1, pp. 1–17, Feb. 2017.
[43] S. Sondhi and Y. V. Hote, "Fractional order PID controller for load frequency control," *Energy Convers. Manage.*, vol. 85, pp. 343–353, Sep. 2014.
[44] E. Sahin, "Design of an optimized fractional high order differential feedback controller for load frequency control of a multi-area multi-source power system with nonlinearity," *IEEE Access*, vol. 8, pp. 12327–12342, 2020.
[45] M. Özdemir and D. Öztürk, "Comparative performance analysis of optimal PID parameters tuning based on the optics inspired optimization methods for automatic generation control," *Energies*, vol. 10, no. 12, p. 2134, Dec. 2017.
[46] M. G. Hemeida, A. A. Ibrahim, A.-A.-A. Mohamed, S. Alkhalaf, and A. M. B. El-Dine, "Optimal allocation of distributed generators DG based manta ray foraging optimization algorithm (MRFO)," *Ain Shams Eng. J.*, Aug. 2020.
[47] A. Fathy, H. Rezk, and D. Yousri, "A robust global MPPT to mitigate partial shading of triple-junction solar cell-based system using manta ray foraging optimization algorithm," *Sol. Energy*, vol. 207, pp. 305–316, Sep. 2020.

EMAD A. MOHAMED received the B.Sc. and M.Sc. degrees in electrical power engineering from Aswan University, Aswan, Egypt, in 2005 and 2013, respectively, and the Ph.D. degree in electrical power engineering from the Kyushu Institute of Technology, Japan, in 2019.

From November 2007 to August 2013, he was a Demonstrator with the Department of Electrical Engineering, Aswan Faculty of Engineering, Aswan University, where he was an Assistant Lecturer, from 2013 to 2015. He was a Research Student with Kyushu University, Japan, from April to October 2015, where he has been an Assistant Professor, since May 2019. He was with the Faculté des Sciences et Technologies, Université de Lorraine, France–1, by the Master Mobility Scholarship. The scholarship was sponsored by the FFEEBB ERASMUS MUNDUS. His current research interests include applications of superconducting power devices, power system stability, and reliability and protection

EMAD M. AHMED (Senior Member, IEEE) received the B.Sc. and M.Sc. degrees from Aswan University, Egypt, in 2001 and 2006, respectively, and the Ph.D. degree from Kyushu University, Japan, in 2012.

He was a member of Aswan Power Electronics Applications Research Center (APEARC), from 2012 to 2018. In 2018, he joined the Aswan Wireless Communication Research Center (AWCRC). He is currently working as an Associate Professor with the Department of Electrical Engineering, Faculty of Engineering, Aswan University. Moreover, he is on leave at the Faculty of Engineering, Jouf University, Saudi Arabia. His current research interests include applied power electronics, especially in renewable energy applications, micro-grids, fault tolerant control, and battery management systems. He is a member of the IEEE Power Electronics Society (PELS), the IEEE Industrial Electronics Society (IES), and the IEEE Power and Energy Society (PES).

AHMED ELMELEGI received the B.Sc. and M.Sc. degrees in electrical power engineering from Aswan University, Aswan, Egypt, in 2005 and 2019, respectively. He joined Upper Egypt Electricity Distribution Company, Ministry of Electricity and Renewable Energy, Aswan, in 2007. His current research interests include applied power electronics in renewable energy applications, multi-level inverters, and micro-grids.

MOKHTAR ALY (Member, IEEE) received the B.Sc. and M.Sc. degrees in electrical engineering from Aswan University, Aswan, Egypt, in 2007 and 2012, respectively, and the Ph.D. degree from the Department of Electrical Engineering, Faculty of Information Science and Electrical Engineering, Kyushu University, Japan, in 2017.

In 2008, he joined the Department of Electrical Engineering, Aswan University, as an Assistant Lecturer, where he has been an Assistant Professor with the Faculty of Engineering, since 2017. He is currently a Postdoctoral Researcher with the Solar Energy Research Center (SERC-Chile), Universidad Técnica Federico Santa María, Chile. His current research interests include reliability of power electronics systems, especially in renewable energy applications, multi-level inverters, fault tolerant control, electric vehicles, and light emitting diode (LED) lamp drivers. He is a member of IEEE Power Electronics Society (PELS), IEEE Industrial Electronics Society (IES), and IEEE Power and Energy Society (PES).

OSAMA ELBAKSAWI received the B.Sc. degree (Hons.) in electrical engineering from the Faculty of Engineering, Suez Canal University, Egypt, in 1996, and the M.Sc. and Ph.D. degrees in power and electrical machines from Suez Canal University, Egypt, in 2002 and 2009, respectively. From 2010 to 2014, he worked as an Assistant Professor of Electrical Engineering with the Faculty of Engineering, Port-Said University. Since 2014, he has been working as an Assistant Professor with the College of Engineering, Jouf University. His research contributions include the area of power systems and electrical machines, which can be classified into the following topics: control of power systems, different optimization algorithms, load frequency control, micro-grid systems, drive systems, renewable energy conversion for PV, and wind systems.

AL-ATTAR ALI MOHAMED received the B.Sc., M.Sc., and Ph.D. degrees in electrical engineering from Aswan University, Aswan, Egypt, in 2010, 2013, and 2017, respectively. He is currently an Assistant Professor with the Department of Electrical Engineering, Faculty of Engineering, Aswan University. His research interests include the area of analysis and design of power systems, optimization and controls, renewable energy applications, micro-grids, electric vehicles, and energy storage systems.